DEFECT COMPLEXES IN SILICON: ELECTRONIC STRUCTURES AND POSITRON ANNIHILATION

Mikko Hakala

Laboratory of Physics
Helsinki University of Technology

Fysiikan laboratorio
Teknillinen korkeakoulu

DISSERTATION 111 (2001)

DEFECT COMPLEXES IN SILICON: ELECTRONIC STRUCTURES AND POSITRON ANNIHILATION

Mikko Hakala

Laboratory of Physics
Helsinki University of Technology
Espoo, Finland

Dissertation for the degree of Doctor of Science in Technology to be presented with due permission of the Department of Engineering Physics and Mathematics for public examination and debate in Auditorium E at Helsinki University of Technology (Espoo, Finland) on the 9th of February, 2001, at 12 o'clock noon.

Dissertations of Laboratory of Physics, Helsinki University of Technology
ISSN 1455-1802

Dissertation 111 (2001):
Mikko Hakala: Defect Complexes in Silicon: Electronic Structures and Positron Annihilation
ISBN 951-22-5310-0 (print)
ISBN 951-22-5311-9 (electronic)

OTAMEDIA OY
ESPOO 2001

Abstract

In silicon processing technology one of the most important current objectives is to achieve a controlled impurity doping in the crystal. Point defects and defect complexes present in the crystal influence in an important way the electrical activity and the diffusion properties of the dopants. In this thesis, defect complexes in silicon are studied by using quantum-mechanical electronic-structure calculations and by modeling positron annihilation experiments.

The electronic-structure calculations are based on the density-functional theory and its state-of-the-art implementations, such as a plane-wave pseudopotential computer code. For the calculation of the momentum density of annihilating electron-positron pairs a new method is presented and tested. It is based on a two-particle description of the correlated pair so that the contact density depends explicitly on the whole spatial distribution of the electron state in question. The new method is found to be superior to the state-independent methods for the momentum density and provides a basis for identifying defect complexes with different chemical surroundings from their momentum distribution fingerprint.

In this work, the computational methods are used to study the positron annihilation characteristics at small vacancy clusters in silicon and the properties of typical dopant atoms, which include arsenic and boron. In highly arsenic-doped silicon an electrically inactive defect complex consisting of a vacancy decorated by three arsenic atoms is identified. In boron-doped silicon the defect structures containing one boron atom are analyzed and an estimate is given for the activation energy of boron diffusion.

Preface

The thesis has been prepared in the Laboratory of Physics at the Helsinki University of Technology during the years 1996-2000.

I wish to thank my supervisor Academy Prof. Risto Nieminen for providing the opportunity for carrying out the research, and for the encouragement and ideas during the work. Prof. Martti Puska, Dr. Bernardo Barbiellini, Prof. Kimmo Saarinen, and Dr. Matti Alatalo have been the foremost collaborators, for whom I wish to express my gratitude. I am indebted to Dr. Sami Pöykkö, Dr. Tomi Mattila, Dr. Ari P. Seitsonen, and Prof. Kari Laasonen for the computational guidance. I want to thank Dr. Timo Korhonen, Dr. Alfred Manuel, Dr. Catherine Corbel, Dr. Hannu Kauppinen, M.Sc. Jaani Nissilä, and Prof. Pekka Hautojärvi for the collaboration.

Thanks are due to all the colleagues and the personnel in the laboratory, without whom the work could not have been accomplished. I am grateful to my parents, my sister, and my grandparents, as well as friends, who have given me joy and support during the work.

Finally, I acknowledge the generous computing resources of the Center for Scientific Computing.

Espoo, January 2001

Mikko Hakala

Contents

List of publications

This thesis consists of an overview and the following publications:

I M. Alatalo, B. Barbiellini, M. Hakala, H. Kauppinen, T. Korhonen, M. J. Puska, K. Saarinen, P. Hautojärvi, and R. M. Nieminen, *Theoretical and experimental study of positron annihilation with core electrons in solids*, Phys. Rev. B. **54**, 2397-2409 (1996).

II B. Barbiellini, M. Hakala, M. J. Puska, R. M. Nieminen, and A. A. Manuel, *Correlation effects for electron-positron momentum density in solids*, Phys. Rev. B. **56**, 7136-7142 (1997).

III M. Hakala, M. J. Puska, and R. M. Nieminen, *Momentum distributions of electron-positron pairs annihilating at vacancy clusters in Si*, Phys. Rev. B. **57**, 7621-7627 (1998).

IV K. Saarinen, J. Nissilä, H. Kauppinen, M. Hakala, M. J. Puska, P. Hautojärvi, and C. Corbel, *Identification of vacancy-impurity complexes in highly n-type Si*, Phys. Rev. Lett. **82**, 1883-1886 (1999).

V M. Hakala, M. J. Puska, and R. M. Nieminen, *First-principles calculations of interstitial boron in silicon*, Phys. Rev. B **61**, 8155-8161 (2000).

The author has had an active role in all the phases of the research reported in this thesis. He has been involved in the planning of the calculations, the development of the computer programs, and the interpretation of the results. The author has written Publications III and V, and contributed actively to the writing of the other papers. He has performed all the calculations except the LMTO-ASA calculations in Publications I and II. He has been responsible for developing the computer programs for the positron calculations needed in Publications I-IV.

Additionally, the following closely related papers have been published during this work:

B. Barbiellini, M. J. Puska, M. Alatalo, M. Hakala, A. Harju, T. Korhonen, S. Siljamäki, T. Torsti, and R. M. Nieminen, *Correlation effects for positron annihilation with core and semicore electrons*, Appl. Surf. Sci. **116**, 283-286 (1997).

J. Gebauer, M. Lausmann, T. E. M. Staab, R. Krause-Rehberg, M. Hakala, and M. J. Puska, *Microscopic identification of native donor Ga-vacancy complexes in Te-doped GaAs*, Phys. Rev. B. **60**, 1464-1467 (1999).

M. Hakala, M. J. Puska, and R. M. Nieminen, *Theoretical studies of interstitial boron defects in silicon*, Physica B **273-274**, 268-270 (1999).

1 Introduction

Chemical purity and a suitable intrinsic carrier density make single-crystal silicon the main material for the fabrication of semiconductor components [1]. The desired electrical conductivity is achieved by doping silicon with impurity atoms. One of the challenges is the understanding of how these dopant atoms interact with the native and introduced lattice defects. The parameter-free (*ab initio*) theoretical methods are in this respect superior tools. They give an accurate physical insight and can be used to extract necessary parameter values for the higher-level simulations. The computational cost of these methods restricts their use to the study of point defects, instead of extended lattice defects. The main interests are the formation and structure of the intrinsic point defects and their complexes with the impurity atoms. This data can be then used to study the diffusion and the electrical activity of the dopants.

In this thesis, point defects and defect complexes are studied using electronic structure calculation methods and positron annihilation spectroscopy. The specific feature of the positron annihilation spectroscopy in defect studies is the sensitivity of the positron to open-volume defects. This is due to the fact that the positron finds an energy minimum in the region where the ionic potential is smaller than average. As the positron finally annihilates with an electron, the energy and time distribution of the produced gamma radiation convey information on the local electron density. This makes an accurate defect identification possible. In this thesis the approach is purely computational, *i.e.*, the relevant physical quantities are calculated from the theory and compared with the existing experimental values. The electronic structure methods are becoming standardized and can be used rather straightforwardly. On the contrary, theoretical methods for the positron state and the annihilation characteristics have not been examined that much, and new methods have been developed during this thesis work.

Arsenic and boron are standard dopants in silicon processing [2]. The shrinking component size in the CMOS (Complementary Metal-Oxide-Semiconductor) technology sets new challenges to the process simulators [3]. One has to determine accurately the spatial distribution of the dopant atoms. Highly arsenic-doped silicon has been found to exhibit a saturation of the carrier concentration [2, 4]. In the case of boron the ion implantation has been found to lead to transient-enhanced diffusion and clustering [5]. The atomistic mechanisms in both of the cases are not completely understood.

The first part of the thesis is concerned with improving the theoreti-

cal methods for the positron state and the annihilation characteristics. In Publication I a theoretical model for the momentum density of annihilating electron-positron pairs is formulated and tested in the case of core electrons in a solid. Various metals and elemental and compound semiconductors are used as test cases. Publication II extends the model to the valence-electron annihilation. Copper and gallium arsenide are used as test cases. Publication III studies the annihilation characteristics of small vacancy clusters (1-5 vacancies) in silicon. The latter part of the thesis is concerned with the behavior of the dopants in silicon. Publication IV concentrates on the identification of defects playing a role in the arsenic deactivation mechanism in highly doped silicon. Finally, in Publication V the boron-related point defects and the boron diffusion mechanism in silicon are studied.

The rest of the overview is organized as follows. Section 2 reviews the theory and computational methods for the electronic structure, the positron state, and the positron annihilation characteristics. Section 3 gives a brief introduction to the properties of native defects and dopants in silicon. The achieved results are reviewed in Section 4. Section 5 concludes the work.

2 Theory

2.1 Electronic structure

In this work the electronic structure of condensed-matter systems is solved within the density-functional theory (DFT) [6, 7]. In DFT, the many-body wave function of the interacting electrons is solved in a one-particle form. The many-body effects are taken into account by using approximative exchange and correlation energies, and corresponding potentials. DFT is used widely in today's materials modeling [8].

DFT is based on the theorem by Hohenberg and Kohn [6], according to which the correct ground-state energy of an interacting electron gas in an external potential can be determined by minimizing a functional of the electron density. Kohn and Sham [7] then showed how to transform the original many-particle problem to effective one-particle equations. In this formalism the total energy of a system which contains electrons in an external potential due to the nuclei is written as

$$\begin{aligned} E[n] &= T_0[n] + \frac{1}{2}\int d\mathbf{r}\int d\mathbf{r}'\frac{n(\mathbf{r})n(\mathbf{r}')}{|\mathbf{r}-\mathbf{r}'|} - \int d\mathbf{r} V_{nuc}(\mathbf{r})n(\mathbf{r}) \\ &\quad + E_{nuc}(\{\mathbf{R}_I\}) + E_{\mathrm{xc}}[n]. \end{aligned} \tag{1}$$

Above $T_0[n]$ is the kinetic energy of the noninteracting electrons (n denotes the electron density distribution). The second term is the Hartree energy of the electron-electron Coulomb interactions. The third term is the energy of the Coulomb interaction of the electrons with the system of the positive nuclei with V_{nuc} denoting the potential of the nuclei. E_{nuc} is the Coulomb energy of the nucleus-nucleus interactions, where the set $\{\mathbf{R}_I\}$ denotes the nuclear coordinates. $E_{\mathrm{xc}}[n]$ is the exchange-correlation energy, which takes into account the effects due to the many-body character of the actual wave function of the electronic system. Atomic units are used, *i.e.*, $\hbar = m_e = e = 1$, the length is given in Bohr radii and the energy in Hartrees ($1\ a_0 = 0.529177 \cdot 10^{-10}$ m and 1 Ha = 27.2116 eV, respectively).

The explicit functional form for the exchange and correlation energy $E_{\mathrm{xc}}[n]$ is one of the characteristic features of DFT. If this term were known, DFT would be an exact theory. However, this is not the case for most systems of interest. In the case of solids the local-density approximation (LDA) is the most common solution. In the LDA $E_{\mathrm{xc}}[n]$ is written as

$$E_{\rm xc}[n] = \int d\mathbf{r}\ \epsilon_{\rm xc}(n(\mathbf{r}))n(\mathbf{r}), \tag{2}$$

where $\epsilon_{\rm xc}(n(\mathbf{r}))$ is a sum of the exchange and correlation energies for one electron in a homogeneous electron gas. The exchange part $\epsilon_{\rm x}(n)$ is the average change in energy per electron due to the antisymmetry requirement of the many-particle wave function. It is obtained from the Hartree-Fock theory of free electrons [9]. For the correlation energy $\epsilon_{\rm c}(n)$ Ceperley and Alder [10] have calculated data for various electron densities with quantum Monte Carlo methods. In this work a parametrization by Perdew and Zunger [11] is used. Other forms for $E_{\rm xc}[n]$ exist, based on *e.g.* density gradients, but they are not used in this work.

The electron density is constructed from one-particle wave functions ψ_i as

$$n(\mathbf{r}) = \sum_i f_i |\psi_i(\mathbf{r})|^2, \tag{3}$$

where the sum is over the occupied electron states, and f_i denotes the occupation number of the state. The wave functions are required to be orthogonal.

The Kohn-Sham one-electron equations are obtained by varying the total-energy functional (Eq. (1)) with respect to ψ_i^*. This leads to the equations

$$(-\frac{1}{2}\nabla^2 + V_{eff}(\mathbf{r}))\psi_i(\mathbf{r}) = \epsilon_i\psi_i(\mathbf{r}), \tag{4}$$

where the effective potential V_{eff} is

$$V_{eff}(\mathbf{r}) = -V_{nuc}(\mathbf{r}) + \int d\mathbf{r}'\ \frac{n(\mathbf{r}')}{|\mathbf{r}-\mathbf{r}'|} + \frac{\delta[n(\mathbf{r})\epsilon_{\rm xc}(n(\mathbf{r}))]}{\delta n(\mathbf{r})}. \tag{5}$$

The first two terms in Eq. (5) are the Coulomb potential of the nuclei and the electron density, respectively, and the last term the exhange-correlation potential. The functions ψ_i are thus the noninteracting solutions of the Schrödinger equation with the effective potential of Eq. (5). It should be stressed that in DFT the only physically meaningful quantitities are the

electron density and the total energy. The one-particle wave functions ψ_i and the corresponding energy eigenvalues ϵ_i are in this respect only auxiliary functions, with no rigorous physical content. However, in many cases these wave functions and eigenvalues have turned out to be successful in interpreting measured quasiparticle spectra (*e.g.* photoemission spectra). The legitimacy of this identification is a subject of discussion and development (see, for example, Ref. [12]). The GW method [13] and the screened-exchange (sX-) LDA [14] are examples of methods beyond the standard DFT for calculating the excited states.

There are several ways to implement DFT for calculating the electronic structure of a solid. In this thesis the plane-wave pseudopotential method [15] is used (computer code FINGER [16]). The main approximations and features of the method are as follows: The solid is built of supercells, *i.e.*, large unit cells that contain the studied configuration (crystalline or non-crystalline). The supercell is repeated in space by using periodic boundary conditions in order to simulate the infinite solid. This approximation gives rise to finite-size effects through the elastic, electronic, and electrostatic interactions between the neighboring supercells.

Due to periodicity, the valence electron wave functions can be calculated as Bloch waves. The cell-periodic part of the Bloch wave is expanded in a plane wave basis set. The numerical accuracy of the valence electron density is controlled by a chosen kinetic-energy cutoff of the plane wave set and a chosen wave vector (*i.e.*, **k**-point) sampling. In the atomic core region the expansion requires a lot of basis functions due to the orthogonality of the valence electron wave functions against the core electron wave functions. On the other hand, the role of the core electrons is altogether often negligible in the chemical bonds of the solids. Therefore, to simplify the calculation and reduce the number of the plane waves needed, the so-called pseudopotential approximation [17] can be used.

The pseudopotential replaces the potential of the nuclei and the core electrons by a smoother and weaker potential. The corresponding wave functions, called pseudo wave functions, have no radial nodes in the core region and require less plane waves in the expansion. Outside the core region the pseudopotential is constructed to reproduce the correct behavior of the pseudo wave functions, *i.e.*, the amplitudes and the reference energies of the pseudo and all-electron wave functions must match. Coupled to the requirement of norm conservation, this construction conserves the scattering properties of the all-electron potential. The non-norm-conserving pseudopotentials are another approach to further reduce the number of plane waves

[18].

The exchange-correlation energy between the valence and core electrons is included in the pseudopotential energy as a term which depends linearly on the valence density. Since for some elements this is too crude an approximation, an explicit evaluation of $E_{\rm xc}$ in terms of the total electron density may be required. This is done by redefining the pseudopotential; the procedure is called the nonlinear core-valence exchange-correlation scheme [17, 19].

In the optimization of the electronic and ionic structures the Born-Oppenheimer approximation is used, *i.e.*, the electron and the ion dynamics are decoupled due to the large mass difference of the particles. In the minimization one solves first the electronic structure for a given initial configuration. The electron wave functions are iterated until the self-consistency of Eqs. (3) - (5) [20]. The ions are then moved according to the Hellmann-Feynman forces [15],

$$\mathbf{f}_I = -\frac{\partial E}{\partial \mathbf{R}_I}, \tag{6}$$

after which the electronic structure is reoptimized. The loop is repeated until the forces have converged [21].

Imperfections in an otherwise perfect crystalline solid cause a local rearrangement of the electronic density. For example, in the case of the lattice vacancy in silicon, four covalent electron bonds are broken and they rearrange via hybridization. The electronic states resulting from the hybridization can be described as linear combinations of atomic orbitals (LCAO). The specific feature of a defect in a nonmetallic system is its ability to have several charge states. This is due to the fact that the electrons occupy spatially localized states of the defect. Furthermore, the occupation of these states can lead to a symmetry-lowering Jahn-Teller distortion, which is due to a splitting of a degenerate defect level. Another related effect is the so-called negative-U property: an increase in the Coulomb energy due to the addition of a second electron to a singly occupied localized orbital is overcome by a decrease of energy due to a strong ionic relaxation [22]. The effective result is a lower total energy.

The semiconductor band gap E_g in DFT can be calculated as a difference between the ionization potential and the affinity energy, which can be both written in terms of ground-state energies. This leads to the form [8]

$$E_g = \Delta\epsilon + \Delta, \tag{7}$$

where $\Delta\epsilon$ is the difference of the Kohn-Sham eigenvalues between the calculated bottom of the conduction band and the top of the valence band, and Δ is the possible discontinuity in the exchange-correlation potential. In the LDA, $\Delta \equiv 0$ and the eigenvalue band gap is about half the experimental value. It is not well known to which extent the discrepancy is due to the discontinuity or the LDA itself [8]. Attempts to correct for these deficiencies include the above-mentioned sX-LDA [14] and GW methods [13]. Moreover, it should be noted that the use of the Kohn-Sham LDA eigenvalues for the position of the defect ionization levels in the gap is not valid [8]. A way to obtain an estimate for a defect level is to use the total (or formation) energy differences, since the total energies are ground state properties which can be used in the so-called ΔSCF calculations [8].

The formation energy of a defect in a semiconductor is defined as [23, 24]

$$E_f^q = E_D^q + q(E_v + \mu_e) - \sum_s n_s \mu_s, \tag{8}$$

where E_D^q is the total energy of the supercell with a defect D in the charge state q. The second term takes into account the transfer of charged particles, electrons or holes, to the defect from an electron reservoir with a chemical potential (Fermi level) $E_v + \mu_e$. E_v is the valence band maximum and μ_e the position of the chemical potential in the band gap relative to E_v. n_s is the number of atoms of type s in the supercell and μ_s the chemical potential of an atom of type s. The chemical potential of an atom is the total energy/atom in a typical chemical environment. For the supercells containing charged defects, E_v must be calculated indirectly by using a correction to the value in a perfect supercell. The corrected E_v for a defect calculation is [25, 26]

$$E_v = E_{v(\text{bulk})} + [V_{ave(\text{defect})} - V_{ave(\text{bulk})}], \tag{9}$$

where $V_{ave(\text{bulk})}$ is the average potential in a bulk supercell, and $V_{ave(\text{defect})}$ the value in the defect supercell, calculated far from the position of the defect.

The ionization level $\epsilon^{q/q'}$ of a defect is defined as the position of the electron chemical potential when the two charge states, q and q', of a defect have the same formation energy:

$$E_D^q + q[E_v^q + \epsilon^{q/q'}] = E_D^{q'} + q'[E_v^{q'} + \epsilon^{q/q'}]. \tag{10}$$

Finally, in calculating the energies of charged defects one needs to add a neutralizing, constant background charge to the supercell to avoid divergences. This leads to an unphysical electrostatic interaction between the charged defect and the added background charge. Makov *et al.* [27] have proposed a correction for the electrostatic energy,

$$\Delta E = \frac{q^2\alpha}{2L\epsilon} + \frac{2\pi qQ}{3L^3\epsilon} + O(L^{-5}), \tag{11}$$

where q is the charge state of the defect, α the Madelung constant, ϵ the static dielectric constant, L the linear dimension of the supercell and Q the quadrupole moment of the charge distribution of the defect. The practice of using the correction is as yet unestablished.

2.2 Positrons in solids

The positron is the antiparticle of an electron: its charge has the magnitude of the electron, but it is positive in sign. Radioactive nuclei are typical positron sources. Solid state positron spectroscopy is based on the annihilation of positrons with electrons (for a review, see Refs. [28, 29]). The annihilation produces gamma radiation, whose energy spectrum reflects the electron distribution in the sample. The most important annihilation process is the two-gamma annihilation. In this process the collinearity between the quanta is deviated due to the momentum of the center-of-mass of the annihilating electron-positron pair. The deviation can be measured with the one- or two-dimensional angular correlation of the annihilation radiation (1D-, 2D-ACAR) methods and with the Doppler broadening techniques. In addition, the lifetime of the positron in a sample depends on the average electron density at the site of the annihilating positron.

Positrons can be injected in the sample either directly from a radioactive source, in which case they have a continuous energy distribution from zero to $\sim$1 MeV, or as monoenergetic beams with energy typically in the range 0-40 keV. The mean penetration depth depends on the material. For positrons

obtained directly from a radioactive source the mean penetration depth is of the order of 10-100 μm, whereas for monoenergetic positrons the range is typically from 1 nm to a few μm. In the sample positrons rapidly lose their initial kinetic energy first via ionization processes, then via electron-hole excitations, and finally via phonon scattering. After losing the excess energy positrons live in thermal equilibrium with the ions and the electrons of the sample. The thermalization time of the positron is short compared with the typical lifetimes [30] and can be omitted in most cases.

In thermal equilibrium the positron state develops as a diffusion process in real space. The positron scatters from phonons, electrons and defects, of which the phonons give the dominant contribution [31]. The average diffusion length at room temperature is of the order of 1000 Å. In the case of periodic crystals and normal experimental conditions there is only one positron in the sample at a time. Its thermalized state can be described as a $\mathbf{k} = 0$ Bloch state. Due to Coulomb repulsion the positron wave function is mainly located in the interstitial region of the crystal far from the positive nuclei.

Localized positron states can be formed at open-volume crystal defects (*e.g.* vacancies, voids, or dislocations). In the case of semiconductors and insulators the positron can be weakly bound by negatively charged defects (notably impurity ions). In a localized state the positron energy eigenvalue is lower than in a delocalized state. In open-volume defects the Coulomb repulsion is diminished due to the missing nuclear charge and the positron is localized with a binding energy of the order of 1 eV. In the case of negative ions the positron forms an effective-mass state around the negative ion, the binding energy of which is of the order of 10-100 meV.

In solids several kinds of traps may be present. The competition between trapping and transport of the positron distribution function can be analyzed on the basis of transition rates calculated from the Fermi Golden Rule. Simple models for trapping and annihilation have been developed to analyze the experimental data.

2.3 Two-component density-functional theory

The two-component density-functional theory (TCDFT) [32] describes the ground state of a system that consists of positrons and electrons in an external potential. The total energy of the system as a function of the average electron and positron densities (n_- and n_+, respectively) is written as

$$
\begin{aligned}
E[n_-, n_+] &= F[n_-] + F[n_+] - \int d\mathbf{r}\; V_{nuc}(\mathbf{r})[n_-(\mathbf{r}) - n_+(\mathbf{r})] \\
&\quad - \int d\mathbf{r} \int d\mathbf{r}'\; \frac{n_-(\mathbf{r}) n_+(\mathbf{r}')}{|\mathbf{r} - \mathbf{r}'|} + E_{\rm c}^{e-p}[n_-, n_+] \\
&\quad + E_{nuc}(\{\mathbf{R}_I\}),
\end{aligned} \tag{12}
$$

where $F[n]$ reads as

$$
F[n] = T_0[n] + \frac{1}{2} \int d\mathbf{r} \int d\mathbf{r}'\; \frac{n(\mathbf{r}) n(\mathbf{r}')}{|\mathbf{r} - \mathbf{r}'|} + E_{\rm xc}[n] \tag{13}
$$

for the electrons or the positrons. The external potential of the system is assumed to be due to the nuclei. In Eq. (13) $T_0[n]$ is the kinetic energy of the noninteracting electrons or positrons as in Eq. (1). The second and the third term are the Hartree and the exchange-correlation energies of the electrons or the positrons. In Eq. (12) the third term is the Coulomb energy of the electrons and the positrons in the potential of the nuclei. The fourth term is the Hartree energy of the interacting electron and the positron densities. $E_{\rm c}^{e-p}[n_-, n_+]$ is the correlation energy describing the electron-positron many-body interactions. Finally, E_{nuc} is the Coulomb energy of the nucleus-nucleus interactions as in Eq. (1). Puska *et al.* [33] have presented a two-dimensional interpolation form for $E_{\rm c}^{e-p}$ in the local-density approximation (LDA). The numerical form is based on the hypernetted-chain calculations by Lantto [34]. For the special case of the zero-positron-density limit, the interpolation form is that given by Boroński and Nieminen [32], based on the many-body calculations by Arponen and Pajanne [35].

For one positron in the crystal the positron density is written as

$$
n_+(\mathbf{r}) = |\psi_+(\mathbf{r})|^2, \tag{14}
$$

where ψ_+ is the positron ground state wave function. The electron density n_- is given in Eq. (3). The generalized Kohn-Sham equations read as

$$
(-\frac{1}{2}\nabla^2 + [\frac{\delta E_{\rm xc}[n_-]}{\delta n_-(\mathbf{r})} - \phi(\mathbf{r}) + \frac{\delta E_{\rm c}^{e-p}[n_-, n_+]}{\delta n_-(\mathbf{r})}])\psi_i(\mathbf{r}) = \epsilon_i \psi_i(\mathbf{r}), \tag{15}
$$

$$
(-\frac{1}{2}\nabla^2 + [\frac{\delta E_{\rm xc}[n_+]}{\delta n_+(\mathbf{r})} + \phi(\mathbf{r}) + \frac{\delta E_{\rm c}^{e-p}[n_-, n_+]}{\delta n_+(\mathbf{r})}])\psi_+(\mathbf{r}) = \epsilon_+ \psi_+(\mathbf{r}), \tag{16}
$$

where $\phi(\mathbf{r})$ is the total Coulomb potential of the system,

$$\phi(\mathbf{r}) = \int d\mathbf{r}' \frac{-n_-(\mathbf{r}') + n_+(\mathbf{r}') + n_0(\mathbf{r}')}{|\mathbf{r} - \mathbf{r}'|}. \tag{17}$$

Above n_0 denotes the external background charge density due to the nuclei. Equation (16) can be simplified if the correction for the positron self-interaction is made: in the case of one positron the exchange-correlation energy should cancel exactly the self-direct Coulomb energy. Equation (13) for the positron contains then only the term $T_0[n_+]$ and Eq. (16) simplifies accordingly. Eventually, the set of all the equations has to be solved self-consistently.

In the case of a delocalized positron the positron density is everywhere vanishingly small. The electronic structure (Eqs. (15) and (17)) can be solved without the effect of the positron; *i.e.*, $\frac{\delta E_c^{e-p}[n_-,n_+]}{\delta n_-(\mathbf{r})} \to 0$ and $n_+ \to 0$. The effective potential for the positron becomes

$$V_{eff}^+(\mathbf{r}) = \int d\mathbf{r}' \frac{-n_-(\mathbf{r}') + n_0(\mathbf{r}')}{|\mathbf{r} - \mathbf{r}'|} + V_{corr}[n_-], \tag{18}$$

where $V_{corr}[n_-]$ denotes the zero-positron-density limit of $\frac{\delta E_c^{e-p}[n_-,n_+]}{\delta n_+(\mathbf{r})}$.

For a localized positron the practical difficulty of the two-component scheme is its computational demand. In addition, the correlation effects in two-component plasmas may be less accurately known. Therefore the above-mentioned zero-positron-density solution has been also used for the localized positron states. These kind of calculations are often referred to as 'conventional-scheme' calculations. The differences compared to the full TCDFT are small, which is due to the cancellation effects between, for example, the increase of the local average electron density at the positron and the decrease of the contact density [32, 33].

The positron wave function is solved in a real-space point mesh [36]. The defect-defect interaction in the supercell approximation is minimized by using a two-point Brillouin-zone sampling [37]. For the electronic structures within the positron calculations three methods have been used: the plane-wave pseudopotential method (Sec. 2.1), the linear-muffin-tin-orbital method within the atomic-spheres approximation (LMTO-ASA) [38], and the non-self-consistent atomic-superposition method (ATSUP) [36, 39]. In the ATSUP method the electronic structure is solved as the superposition

of the free-atom electron densities. With this method the positron annihilation rates are rather close to those obtained with self-consistent electron densities. The similarity is due to the fact that although the valence electron structure is different in the different methods, the positron density relaxes following the transfer of the electron density.

The positron annihilation rate in the case of vanishing positron density is [30]

$$\lambda = \pi r_0^2 c \int d\mathbf{r}\ n_+(\mathbf{r}) n_-(\mathbf{r}) g[n_-(\mathbf{r})], \tag{19}$$

where r_0 is the classical electron radius and c the speed of light. $g[n_-]$ is the contact value of the electron-positron pair correlation function (also called the contact density) as $n_+ \to 0$. For $g[n_-]$ the LDA interpolation form by Boroński and Nieminen is used [32]. $g[n_-]$ takes into account the pileup of the electrons at the positron, which increases the annihilation rate over the independent-particle model (IPM), for which $g[n_-] \equiv 1$. The positron lifetime τ is the inverse of the annihilation rate, $\tau = \lambda^{-1}$.

Barbiellini *et al.* [40] have developed a generalized gradient approximation (GGA) for the positron states within the zero-positron-density limit. It is based on the gradient expansion of the electronic screening cloud at the positron. The lowest-order gradient correction to the LDA is written as a function of a parameter ϵ, which depends on the electron density variations and the local Thomas-Fermi screening length $(q_{\mathrm{TF}})^{-1}$:

$$\epsilon = |\nabla n_-|^2 / (n_- q_{\mathrm{TF}})^2. \tag{20}$$

The contact density and the positron-electron correlation energy are reformulated using ϵ:

$$g_{\mathrm{GGA}} = 1 + (g_{\mathrm{LDA}} - 1) \exp(-\alpha\epsilon), \tag{21}$$

$$E^{e-p}_{\mathrm{c,GGA}}[n_-(\mathbf{r})] = E^{e-p}_{\mathrm{c,LDA}}[n_-(\mathbf{r})] \exp(-\alpha\epsilon/3), \tag{22}$$

for which there is freedom in choosing the constant α. The value 0.22 is found to give lifetimes in good agreement with experiment, and it is used

throughout the calculations. At the limit $\epsilon = 0$ (uniform electron gas) the model reduces to the LDA and at the limit $\epsilon \to \infty$ (rapid density variations) to the IPM. It should be noted that the GGA scheme uses a different LDA contact density than that by Boroński and Nieminen discussed above. The contact density is based on the data by Arponen and Pajanne (for details, see [40]). The GGA has been found to improve the results for the positron states and the annihilation characteristics. Other models beyond the LDA (*e.g.* the weighted-density approximation, WDA [41, 42]) have not been considered in this work.

2.4 Momentum density of electron-positron pairs

The momentum density of annihilating electron-positron pairs can be written as [30]

$$\rho(\mathbf{p}) = \sum_j \left| \int d\mathbf{r} \ \exp(-i\mathbf{p}\cdot\mathbf{r}) \ \psi_j^{ep}(\mathbf{r},\mathbf{r}) \right|^2 , \tag{23}$$

where $\psi_j^{ep}(\mathbf{r},\mathbf{r})$ is the two-particle wave function when the positron and the electron of state j reside at the same point. The sum is over the occupied core and the valence states. The integral of $\rho(\mathbf{p})$ over the momenta gives the total annihilation rate,

$$\lambda = \frac{\pi r_0^2 c}{(2\pi)^3} \int d\mathbf{p} \ \rho(\mathbf{p}). \tag{24}$$

The two-particle wave function is usually written in a product form

$$\psi_j^{ep}(\mathbf{r},\mathbf{r}) = \psi_+(\mathbf{r})\psi_j(\mathbf{r})\sqrt{g[n_-(\mathbf{r})]}, \tag{25}$$

where $\psi_+(\mathbf{r})$ and $\psi_j(\mathbf{r})$ are the positron and the electron wave functions, solved without the short-range electron-positron correlation effects. The correlation effects are included through the enhancement function $g[n_-]$.

Apart from the independent-particle model ($g[n_-] \equiv 1$), several types of enhancement functions have been developed. The LDA enhancement function by Boroński and Nieminen [32] contains only the dependence on the local electron density. In the GGA model by Barbiellini *et al.* [40] the enhancement function contains also the gradient of the electron density. These

models can be called state-independent models. They are a straightforward application of the formulas discussed in the context of calculating the total annihilation rate. Daniuk *et al.* [43], in addition to the local-density dependence, use a state-selective function. Rubaszek *et al.* [44] have studied a nonlocal state-dependent scheme based on the WDA. A different approach is taken by Sormann [45], who introduces a nonlocal enhancement by taking into account the lattice effects.

In this work a state-dependent model for the annihilating electron-positron pairs is developed (Publications I and II). It is distinguished from the models above by the use of a constant, electron-state-dependent enhancement factor which is calculated from the annihilation rates. The momentum density in this theory becomes

$$\rho(\mathbf{p}) = \sum_j \gamma_j \left| \int d\mathbf{r} \ \exp(-i\mathbf{p}\cdot\mathbf{r}) \ \psi_+(\mathbf{r})\psi_j(\mathbf{r}) \right|^2 , \tag{26}$$

where γ_j is a constant enhancement factor

$$\gamma_j = \lambda_j / \lambda_j^{\mathrm{IPM}} \tag{27}$$

for each electron state. λ_j is the annihilation rate with the state j in the LDA or the GGA model (Eq. (19)).

The theoretical counterparts for the experimental spectra are obtained by integrating the total momentum density along the appropriate crystal directions. The 2D-ACAR spectrum is given by

$$\rho(p_x, p_y) = \int \rho(\mathbf{p}) dp_z, \tag{28}$$

and the 1D-ACAR or the Doppler spectrum is the one-dimensional momentum distribution

$$\rho(p_z) = \int\int \rho(\mathbf{p}) dp_x dp_y. \tag{29}$$

In practice, when comparing the theoretical and the experimental ACAR and Doppler spectra, the spectra are normalized to unity.

The so-called shape parameters S and W of the Doppler spectrum are defined as the relative number of annihilations in chosen momentum windows. They read as

$$S = \frac{A_S}{A_{tot}}, \quad W = \frac{A_W}{A_{tot}}. \tag{30}$$

A_S is the number of annihilations in the range $[0, p_z]$ close to the peak of the spectrum, where the valence-electron annihilation dominates. A_W is the number of annihilations in the range $[p_{z,1}, p_{z,2}]$ corresponding to higher momenta, where the core-electron annihilation dominates. A_{tot} is the total number of annihilations.

3 Point defects and defect complexes in silicon

3.1 Introduction

Impurity doping and dopant diffusion belong to the so-called Front End Of the Line processes in integrated circuit manufacturing [3]. The general problem is control of diffusion and electrical activity of the dopants. The numerical models for these processes range from macroscopic continuum descriptions to microscopic atomic level models. Bridging the gap between the microscopic and the macroscopic scales has become essential for improving the numerical tools for the industrial environment (*e.g.* Technology Computer Aided Design (TCAD) methods). In general, the construction of a model requires identification of the dominant lattice defects and understanding of the interactions between the defects. Due to the complexity of the defect reactions, much of the basic data on defect structures and energetics is still lacking.

Point defects are elementary lattice defects that affect the diffusion and electrical activity of the dopants. They comprise native defects (vacancies, self-interstitials and their agglomerates), dopant atom - native defect complexes, and other impurity atoms. This work considers the identification of small atomic-scale vacancy clusters and the identification and diffusion properties of arsenic and boron, and their defect complexes. Alongside phosphorus, arsenic and boron are the most important donor and acceptor dopants in Si, respectively [3].

3.2 Vacancies and interstitials

Vacancies and interstitials determine to a large extent the diffusion properties of the important dopants. The formation energies of the vacancies and the self-interstitials are $\sim 3{-}4$ eV, and they can exist in various charge states [46, 47]. Their self-diffusion properties provide information on the diffusion mechanisms in the lattice [2]. There are also several fabrication steps in which native defects and their aggregates are created in the lattice. For example, surface oxidation injects interstitials in the lattice [2], whereas the carrier lifetime control, via proton implantation, introduces divacancies [48]. Vacancy aggregation can be expected as a consequence of implant damage and etching [49]. Particularly stable configurations consisting of six and ten vacancies are predicted by theory [50]. Finally, in ion implantation

the interstitials are known to form large, so-called {311} defects [51]: rod-like defects whose length can be several microns and which have widths of typically 1−100 nm. The creation mechanism of the {311} defect is related to the formation of small precursor interstitial aggregates [52].

3.3 Highly arsenic-doped silicon

Highly arsenic-doped silicon (arsenic concentration $\sim 10^{21}\mathrm{cm}^{-3}$) exhibits interesting problems related to electrical activity and anomalous diffusion of dopants. Defect deactivation is found to lead to free carrier saturation at the level of $\leq 5 \times 10^{20}\mathrm{cm}^{-3}$ [4]. The experimental phenomena are as follows [53]: Deactivation is observed as a drop in conductivity after annealing at moderate temperatures ($400 - 500°\mathrm{C}$). Higher temperature annealing ($800 - 1000°\mathrm{C}$) partially reactivates the dopants. The dominant electrically inactive complex is of the type $V - \mathrm{As}_n$, but the value of n is unknown. In heavily doped samples the As atoms must thus rearrange themselves to form these kind of complexes.

On the basis of their *ab initio* calculations, Ramamoorthy and Pantelides [53] have presented a model for the underlying atomic-scale processes. In their model different types of $V_m - \mathrm{As}_n$ complexes play distinct roles. Since the formation energies of $V - \mathrm{As}_n$ ($n > 2$) complexes are negative [53, 54], arsenic deactivation is determined by the defect kinetics.

In Publication IV the different vacancy-impurity complexes are identified by using positron annihilation spectroscopy.

3.4 Electron irradiated boron-doped silicon

Electron irradiation is a method which can be used to create uniform distributions of point defects in a sample. In order to get information on the dominant defect reactions, one can study the behavior of the electrical quantities, *e.g.* carrier concentrations and mobilities. The problem is the thorough identification of the generated defects. For example it might be that the energy levels of a defect are known (*e.g.* from the deep-level transient spectroscopy experiments), but its atomic structure is not.

In boron-doped silicon, electron irradiation produces both boron-interstitial [55, 56, 57] and boron-vacancy complexes [58]. The generation of the defects is briefly as follows [59]. First, electron irradiation produces pairs of silicon vacancies and interstitials. The interstitials are mobile at cryogenic temperatures at least under the electron irradiation condition. Boron-

interstitial complexes are observed as substitutional boron atoms trap silicon interstitials. Boron-vacancy complexes are produced after the isolated silicon vacancies have become mobile at 70-200 K. Both the defects (boron-vacancy and boron-interstitial complex) are able to trap electrons at the gap levels [55, 60] and are unstable at room temperature.

The boron-interstitial complex has drawn attention since it is related to the boron diffusion mechanisms. In Publication V the atomic and the electronic structure of the complex are analyzed.

3.5 Boron diffusion

The diffusivity of boron is sensitive to the presence of silicon interstitials. Their importance can be observed from *e.g.* surface oxidation experiments: oxidation introduces interstitials to the bulk of the material, and as a consequence enhanced diffusion of boron is observed (oxidation-enhanced diffusion, OED) [2]. Another situation when excess silicon interstitials are present is ion implantation. Ion implantation creates defects (interstitials and vacancies) in the target area, which interact with the dopant atoms immediately and during the subsequent heat treatment. Fast diffusion of boron under this condition is called transient-enhanced diffusion (TED). Furthermore, during the implantation, clustering of boron with silicon interstitials is observed, as well as other simultaneous phenomena. These phenomena are coupled to boron diffusion through the fact that they limit the number of the diffusing boron and silicon atoms.

Diffusivity (D^*) in thermal equilibrium can be determined by the Arrhenius form

$$D^* = D_0^* \exp(-Q^*/k_B T), \tag{31}$$

where Q^* is the activation energy of diffusion, T the temperature, and k_B the Boltzmann's constant. The prefactor D_0^* consists of the entropy contributions. If the diffusion is mediated by several mechanisms, the total diffusivity is the sum of the individual components.

The activation energy Q^* can be written

$$Q^* = H^m + H^f, \tag{32}$$

where H^f and H^m are the formation and the migration enthalpy of the diffusing species, respectively. If it is further assumed that the system is at

zero pressure, the formation enthalpy in Eq. (32) is given by the theoretical formation energy value (Sec. 2.1).

For the interstitial-mediated boron diffusion mechanism the reaction can be written as [2]

$$\mathrm{Si}_i + \mathrm{B_{Si}} \rightleftharpoons \mathrm{B}_i. \tag{33}$$

where Si_i denotes the silicon self-interstitial, $\mathrm{B_{Si}}$ the substitutional boron and B_i an interstitial boron configuration. In this mechanism a self-interstitial reacts with the substitutional boron so that the boron atom is kicked to the interstitial region. The *ab initio* calculations by Nichols *et al.* [61] suggest that in the interstitial region B_i diffuses via the tetrahedral and the hexagonal sites. Cowern *et al.* [62, 63, 64] provided experimental evidence for this kick-out mechanism for the long-range interstitial boron migration at low temperatures.

In this work several atomic structures for the interstitial boron in the silicon lattice are studied (Publication V). The results yield an activation energy of diffusion for the kick-out reaction, which can be compared with experiments [2]. The results can be also compared with the other *ab initio* studies. Zhu *et al.* [65, 66] have made *ab initio* calculations for boron diffusion and pairing. They calculated a schematic energy diagram including the diffusion barriers for the kick-out reaction. In the recent studies by Sadigh *et al.* [67] and Windl *et al.* [68] a new mechanism for boron diffusion was found. The mechanism has a somewhat lower diffusion barrier than the kick-out mechanism. According to them the fast diffuser is not the B_i defect but the $\mathrm{B_{Si}}$-Si_i defect. This so-called interstitialcy mechanism can be written schematically as [2]

$$\mathrm{Si}_i + \mathrm{B_{Si}} \rightleftharpoons (\mathrm{Si}_i\mathrm{B_{Si}}). \tag{34}$$

First a silicon interstitial is captured by a substitutional boron to form a ($\mathrm{B_{Si}}$-Si_i) defect. The defect diffuses as a complex with a specific barrier. The activation energy for this mechanism is quite close to that obtained for the kick-out reaction (see Sec. 4.5).

3.6 Boron clustering

Ion implantation is a standard method to introduce dopants in silicon. Implantation creates damage in the target area, and a subsequent heat treat-

ment is necessary to activate the dopants. In the case of boron, ion implantation and thermal annealing are found to lead to a formation of boron clusters. The clustering involves several stages and simultaneous phenomena. The main observation is that at higher implantation doses the peak of the implanted boron profile becomes immobile [69] and electrically inactive [70]. This is explained by clustering, which can be divided into three parts: i) the initial nucleation, ii) the cluster evolution, and iii) the formation of the final stable cluster. The initial nucleation takes place during the implantation and the early stages of the annealing, before boron starts to diffuse [71]. When diffusion has started, no new boron nucleation centers are observed [71].

The clustered boron fraction consists of defects of type B_nSi_m, where n, m denote the number of atoms attached to the cluster. The actual atomic structure of the defect is not known. According to Pelaz *et al.* [71] $n, m < 5$; the larger boron clusters are unstable or there is an energy barrier preventing their formation. Pelaz *et al.* [72] find that the silicon interstitial supersaturation is a prerequisite for boron clustering. As the interstitial supersaturation decreases with annealing, interstitials are released from the boron clusters [72].

Simultaneously with the evolution of the boron clusters, transient-enhanced boron diffusion is observed. As discussed in the previous section, it is driven by the mobile silicon interstitials. Moreover, small silicon clusters are observed, which develop into the so-called {311} defects [52]. For the small silicon clusters deep-level studies [73, 74] and estimates for the formation energy are available [52, 75].

According to experiments, the final stable cluster contains $\sim 3-4$ boron atoms and one silicon atom [76]. The dissociation of these clusters requires high temperatures or long annealing times [77]. Pelaz *et al.* [72] explain the dissociation by a reaction in which thermally generated silicon interstitials interact with the cluster so that boron atoms are released. They also find that the cluster is more stable than the {311} defect.

The evolution of the boron clusters after the ion implantation has been simulated by several groups. Slightly differing results have been obtained. Pelaz *et al.* [71, 72] use a kinetic Monte Carlo code, whose simulation parameters are based on their own diffusion experiments. They propose that the precursor defect is BSi_2, whereas nucleation mechanisms based on the B_iB_{Si} or the B_iB_i defects were found to contradict experiment. The stable cluster was found to comprise three or four boron atoms and approximatedly one silicon interstitial. The B_4Si complex was found to have the largest

binding energy.

Caturla *et al.* [78] have implemented a kinetic Monte Carlo simulator based on unpublished *ab initio* data. In their calculations the B_3Si_2 cluster is unstable, and the stable, immobile and inactive complex is proposed to be B_3Si. Windl *et al.* [79] have recently reported a continuum simulator for boron diffusion and clustering based on *ab initio* data.

Few published *ab initio* data are available for the atomic structures and stabilities of the clusters. These comprise the work by Tarnow [80] and Zhu *et al.* [65, 66], who report calculations for two-boron complexes and a table in Ref. [78], which contains dissociation barriers of a set of clusters. There is thus a lack of consistent data for several types of clusters.

4 Results

4.1 Positron annihilation with core electrons in solids

In Publication I the Schrödinger equation for the two-particle electron-positron system is solved approximately by applying the Pluvinage method [81]. The solution is used to model the momentum distribution of the positron annihilating with the core electrons. In the Pluvinage method the pair wave function is assumed to be a product

$$F(\mathbf{r}_1, \mathbf{r}_2) = G(\mathbf{r}_1, \mathbf{r}_2) f(\mathbf{r}_1, \mathbf{r}_2), \tag{35}$$

where $\mathbf{r}_1$ and $\mathbf{r}_2$ are the position vectors of the electron and the positron, $G(\mathbf{r}_1, \mathbf{r}_2)$ describes the orbital motion of the noninteracting particles in the nuclear potential, and $f(\mathbf{r}_1, \mathbf{r}_2)$ describes the correlated motion of the particles. It is further assumed that the correlated motion depends only on the interparticle separation r_{12}. The pair wave function can be thus written

$$F_j(\mathbf{r}_1, \mathbf{r}_2) = \psi_+(\mathbf{r}_1)\psi_j(\mathbf{r}_2)u_j(r_{12}), \tag{36}$$

where j denotes the electron state with which the positron annihilates. The unknown correlation factor $u_j(r_{12})$ at $r_{12} = 0$ can be related to the orbital annihilation rates λ_j through the integral

$$\lambda_j = \pi r_0^2 c \int d\mathbf{r} |F_j(\mathbf{r}, \mathbf{r})|^2 = \pi r_0^2 c u_j^2(0) \int d\mathbf{r} |\psi_+(\mathbf{r})|^2 |\psi_j(\mathbf{r})|^2. \tag{37}$$

λ_j is calculated in the LDA or the GGA approximation (Eq. (19)). Using the equations (23), (36) and (37) [with $\psi_j^{ep}(\mathbf{r}, \mathbf{r}) \equiv F(\mathbf{r}, \mathbf{r})$ and $\gamma_j \equiv u_j^2(0)$] the momentum distribution becomes that of Eq. (26).

In calculating the momentum distributions for different orbitals the positron wave function at the core region of the atoms of the solid is assumed to be isotropic and of the form of the error function; the paper tabulates the parameters for the studied elements. The free-atom (LDA) wave functions are used for the core electrons [82]. The resulting momentum distributions are spherically symmetric.

Two assumptions in this method need to be kept in mind. Firstly, the use of the DFT-LDA wave functions for the single-atom and crystal electrons.

As discussed in Sec. 2.1, the DFT-LDA wave functions and energy levels are not well-defined physical quantities. However, the empirical evidence shows that the use of these wave functions gives a rather accurate numerical result for the momentum density of the annihilating electron-positron pairs as compared with experiments. Even predictive calculations can be performed. Secondly, the assumption that the correlated motion depends solely on the interparticle separation restricts the use of the method to the cases where the electron screening cloud at the positron is isotropic. The theory is thus not valid *e.g.* for positron states on solid surfaces. The theory also breaks down if the positron localization is stronger than the range of the correlation function $u_j(r_{12})$.

The paper analyzes the differences between the theory and the experiment, and between the IPM, the state-dependent LDA and the state-dependent GGA methods for the momentum distribution. A set of bulk metals and semiconductors are used as the test systems. The reduction of the core annihilation rates in the GGA in comparison with the LDA is found essential for good agreement with experiments. The state-independent LDA with the Boroński-Nieminen enhancement function [32] is demonstrated to lead to unphysical, deteriorating oscillations in the momentum distribution in the case of aluminium.

The characteristic features in the shapes of the Doppler spectra are discussed. Atomic resolution is further demonstrated in the case of semiconductor alloys. Finally, the calculation method is applied to defects in semiconductors. The annihilation characteristics show a good agreement between the theory and the experiment. It is shown that the quantity $(\lambda_c/\lambda)_{\mathrm{defect}}/(\lambda_c/\lambda)_{\mathrm{bulk}}$ (λ_c is the sum of the individual λ_j for the core orbitals) is a good approximation for the parameter $(W_{\mathrm{defect}})/(W_{\mathrm{bulk}})$ (Eq. (30)).

4.2 Correlation effects for electron-positron momentum density

In Publication II the state-dependent model (Sec. 4.1) is used to calculate both the valence and the core part of the momentum density of the annihilating electron-positron pairs. The method is tested against the IPM and the state-independent GGA [40] results. Defect-free Cu and GaAs are used as the test systems. The band structures are calculated with the LMTO-ASA [38] and the plane-wave pseudopotential methods (Sec. 2.1).

The Bloch states in Cu show a mixed *sp* and *d* character. For the *d*-type

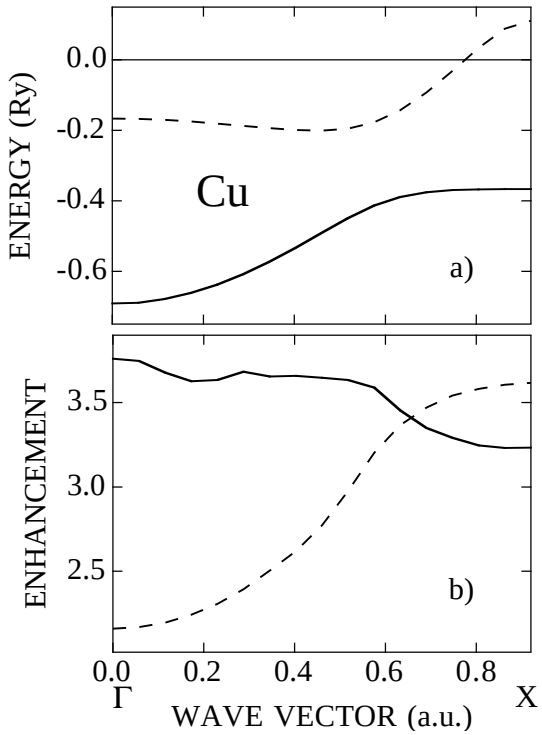

Figure 1: (a) Electron band structure of Cu along the [100] direction in momentum space. Only the bands contributing to the momentum density of annihilating electron-positron pairs are shown. The energy zero coincides with the Fermi level. (b) State-dependent enhancement factor for the bands shown in (a). The solid (dashed) lines in (a) and (b) correspond to each other. Note that the enhancement factors for the states above the Fermi level are unphysical, because they are not occupied.

band the localization of the electron wave functions at the nuclei increases while moving from the bottom of the band towards the top of the band. The increasing localization is seen as a decreasing value of the enhancement factor (Fig. 1). At low energies and energies close to the Fermi level the s character of the states increases, which leads to more delocalized wave functions. The enhancement factor increases accordingly. In addition, it is found that the enhancement factor calculated with the ATSUP-method for the atomic $4s$ wave function agrees well with the s states. The enhancement factor for the atomic $3d$ wave function agrees with the d states in an average fashion.

The theories are compared with the experimental 2D-ACAR spectrum for Cu along the $[1\bar{1}0]$ direction. The inclusion of the correlation effects to the IPM leads to a momentum density more localized close to $\mathbf{p} = 0$. The state-dependent method improves the description in comparison with the state-independent GGA [40] by narrowing the spectrum and by subtracting small oscillations. In comparing the theoretical and the experimental Doppler spectra it is found that a small overestimation in the d state contribution still remains.

Finally, the anisotropy of the 2D-ACAR spectrum of GaAs is calculated as the difference between the cuts along the [110] and [001] directions. The best quantitative agreement with the experiment is obtained with the state-dependent method.

4.3 Positron annihilation at vacancy clusters in silicon

Publication III analyzes the positron states and the annihilation characteristics of perfect bulk Si and the small vacancy clusters containing 1-5 vacancies. The positron lifetimes are calculated at the zero-positron-density limit within the LDA [32]. The momentum distributions are calculated within the state-dependent LDA scheme (Sec. 4.1, 4.2). The analysis is limited to the neutral charge states and to the ideal vacancy structures, *i.e.*, the ionic relaxations are not taken into account.

The gradual increase of the size of the vacancy cluster leads to a systematic change in the positron lifetimes and the momentum distributions. The observations are the following. i) The positron lifetime increases due to the decrease of the average electron density at the annihilating positron. ii) The anisotropy in the 2D-ACAR spectrum vanishes when the vacancy is larger than the monovacancy. In the monovacancy the positron density spills somewhat into the interstitial region of the lattice and the 2D-ACAR and the Doppler spectra contain a small directional anisotropy as in the case of the perfect bulk crystal. iii) In the Doppler spectrum the localization is seen as a systematic decrease of the magnitude at high momenta. This is due to the decreasing spatial overlap of the positron with the core-electron wave functions of the surrounding ions. iv) At low momenta the Doppler spectrum narrows as the open volume increases. The positron overlaps more weakly with the valence-electron wave functions, which in Si are concentrated in the bonds. This leads to an overlap with electrons with a smaller average momentum, and thus to a narrower spectrum.

The results for the bulk crystal are in a good agreement with expe-

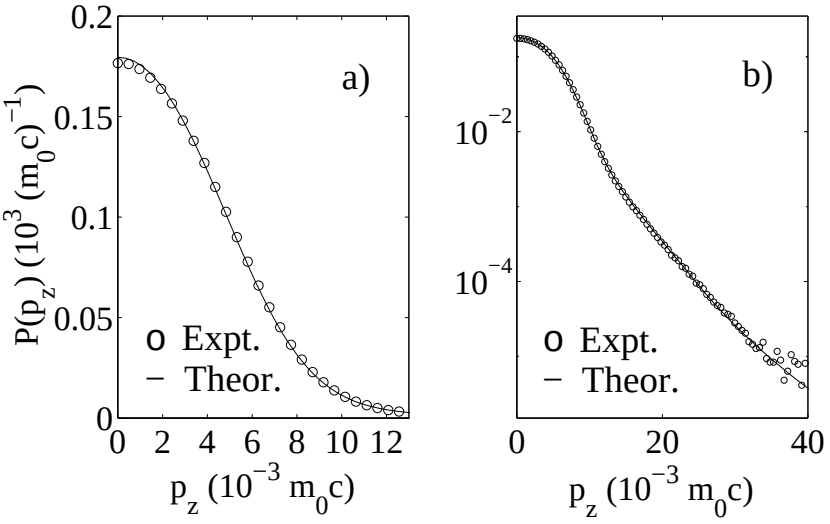

Figure 2: Experimental (Pub. I) (markers) and calculated (lines) positron annihilation probability densities for perfect bulk Si with p_z along the [100] direction: a) linear, b) logarithmic scale. The curves have been convoluted with a Gaussian to mimic the experimental resolution.

riments in both the high and the low momentum regions of the Doppler spectrum (Fig. 2). Moreover, the state-dependent scheme is found to reproduce the directional anisotropy seen in experiments [83], whereas the state-independent LDA of Eq. (25) [32] leads to an overestimation. The annihilation characteristics are in a rather good agreement with the experimental Doppler spectra and the lifetimes in the case of the mono- and the divacancies [48, 84, 85]. Finally, two related experimental studies are worth mentioning: Eichler and Krause-Rehberg [86] studied the effects of the energy resolution and the choice of the energy window on the shape parameters of Eq. (30); Liszkay *et al.* [87] studied the crystal orientation in more detail.

4.4 Vacancy-impurity complexes in arsenic-doped silicon

Publication IV is the outcome of a collaboration project between the author and the experimental positron group at the Laboratory of Physics. The aim of the paper is twofold: i) to show that the positron lifetime and the

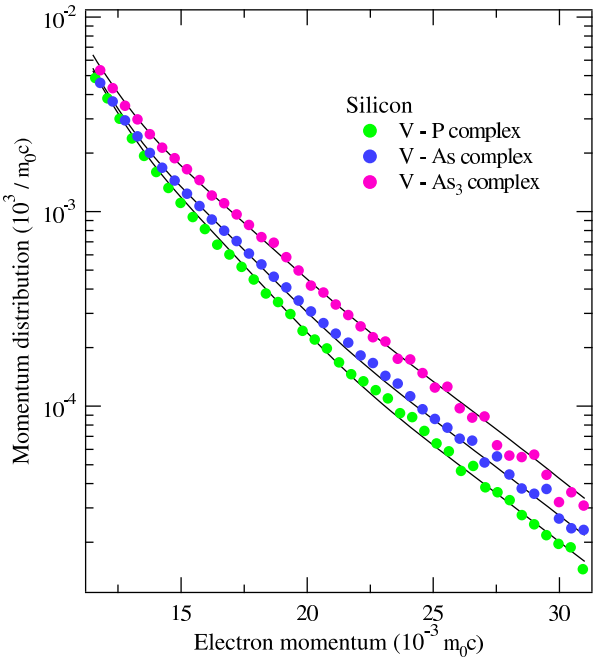

Figure 3: High-momentum part of the electron-positron momentum distribution at the various vacancy-impurity pairs. The experimental results are given by markers and the theoretical results by lines. The data correspond to the $V-\mathrm{P}$ (lowermost curve), $V-\mathrm{As}$, and $V-\mathrm{As}_3$ defects, respectively.

momentum distribution measurements yield quantitative information on the open volume and the atomic surrounding of complexes in silicon; ii) to identify the complexes in electron irradiated and as-grown silicon in order to validate the defect deactivation model by Ramamoorthy and Pantelides [53]. The theoretical calculation method is the same as in Publication III.

The experimental positron lifetimes in as-grown, electron irradiated phosphorous-doped, and electron irradiated arsenic-doped samples are found close to each other and typical of monovacancies (Refs. [85, 88] and Publication III). The experimental Doppler spectra reveal clear differences between the systems at both the low and the high momenta (for the high momenta, see Fig. 3). The effects are due to the increased number of core and valence electrons with which the positron annihilates at the vacancy. To support the identification, theoretical calculations were performed for a set of $V-\mathrm{As}_n$ and $V-\mathrm{P}$ complexes. Ideal atomic structures and neutral charge states were assumed. The positron lifetimes and the momentum distributions fit

well with experiments as exemplified in Fig. 3 for the high momenta of the Doppler spectrum. In electron irradiated Si $V-\mathrm{P}$ and $V-\mathrm{As}$ pairs are identified. In heavily As-doped as-grown Si ([As]=$10^{20}\mathrm{cm}^{-3}$) a native defect $V-\mathrm{As}_3$ is identified.

The findings are in accordance with the defect formation and diffusion mechanisms suggested by Ramamoorthy and Pantelides [53]. The precursor defect for diffusion is the $V-\mathrm{As}$ complex and the fast diffuser is the $V-\mathrm{As}_2$ complex. The formation of $V-\mathrm{As}_2$ is limited by the fact that the average distance between the As atoms must be small enough [89]. In particular, if the doping level is too low, $V-\mathrm{As}_2$ cannot form. At higher doping levels $V-\mathrm{As}_2$ can form and it migrates until gets trapped at a substitutional As to form the electrically inactive $V-\mathrm{As}_3$ complex.

4.5 Interstitial boron in silicon

In Publication V the stable and the metastable interstitial configurations containing one boron atom in an otherwise pure crystal are characterized. The atomic structures, the formation and binding energies and the energy levels of the configurations are investigated. The calculations are performed with the plane-wave pseudopotential method within the spin-polarized density-functional theory [6, 90]. The results are compared with the data provided by electron paramagnetic resonance (EPR) and deep-level transient spectroscopy (DLTS) measurements and with other theoretical results. The energetics of boron diffusion is studied on the basis of the formation energies.

The ground state structure of interstitial boron is depicted in Fig. 4. The ground state consists of a boron atom close to its substitutional site and a silicon atom at a nearby interstitial site. The defect is found to have negative-U properties in accordance with experiments [91], *i.e.*, it is able to trap two electrons so that the second electron is more strongly bound than the first one. The C_{3v} configuration in Fig. 4 corresponds to the case of no electrons in the localized gap states (defect charge +1), and the C_{1h} to the case of two electrons (defect charge -1) in the gap states. The neutral charge state is metastable against the +1 and -1 charges.

Several other metastable configurations for B_i are also found: tetrahedrally coordinated (T), hexagonally coordinated (H), split-interstitial (S), and bond-centered (B) sites. The first three configurations are energetically close (~ 1 eV) to the ground state.

The energetics of boron diffusion is analyzed within the model by Nichols

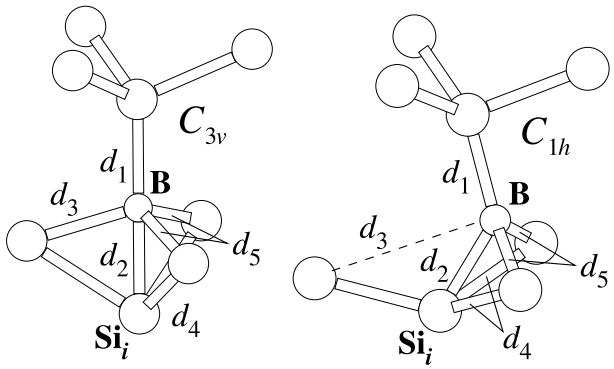

Figure 4: Calculated atomic structure of the B_{Si}-Si_i defect in its two possible configurations.

et al. [61]. The diffusion is assumed to be mediated by silicon interstitials and initiated by a kick-out reaction (Sec. 3.5). The initial configuration is a substitutional boron and a silicon interstitial far from each other. The intermediate configuration is the substitutional boron - interstitial silicon pair (B_{Si}-Si_i). In the interstitial region boron diffuses through the metastable sites, notably the T site. With these configurations the activation energy becomes 3.0 eV + $2\mu_e$ for Fermi level (μ_e) below the midgap, in agreement with experimental values [2] and other first-principles calculations [66, 67, 68]. It should be noted that the results for the activation energy do not practically change if the interstitialcy diffusion mechanism is assumed (Sec. 3.5). This is due to the fact that the metastable configurations are energetically close to the saddle points proposed for the interstitialcy diffusion [67, 68].

If excess silicon interstitials are assumed to be present, as after electron irradiation or ion implantation, the activation energy of boron diffusion lowers to $\sim$ 1 eV for Fermi level below the midgap. Finally, a possible charge-assisted mechanism for boron diffusion is discussed. The mechanism involves capturing of electrons or holes under optical or electrical injection and can lead to a lower activation energy.

5 Summary

In this thesis theoretical methods have been used for calculating the electronic structures and the positron annihilation characteristics of defect complexes in solids. The emphasis has been on various defects in crystalline silicon. The electronic structures have been calculated mainly with a density-functional based plane-wave pseudopotential method. The positron state and the annihilation characteristics have been solved using a two-component density-functional scheme and numerical real-space methods.

The theoretical methods for the positron annihilation characteristics have been improved by the introduction of a new model for the momentum density of the annihilating electron-positron pairs. The model is based on a two-particle description of the annihilating pair and leads to an electron-state-dependent enhancement of the electron density at the positron. In Publication I the model is formulated and tested for the positron annihilating with the core electrons of a solid. In Publication II the model is extended for calculating the positron annihilation with the valence electrons. The model is found to improve the calculated momentum density in comparison with the models where the state dependency is not taken into account. A systematic comparison remains to be done against the other state-dependent models.

Defect complexes in silicon have been studied with respect to their structural and electrical properties and the diffusion mechanisms. Publication III studies the positron annihilation characteristics at small vacancy clusters in silicon. All the changes in the observables can be explained by the degree of the overlap of the positron wave function with the core and the valence electron wave functions. Publication IV shows how the atomic structures of vacancy-impurity complexes are identified in highly arsenic-doped silicon using the theory and the experimental positron annihilation techniques. The formation of the electrically inactive $V - As_3$ defect is observed. In Publication V the electronic structure calculations are used to study interstitial boron defects in silicon. The boron diffusion mechanism is clarified on the basis of the formation energies of the defects.

References

[1] For an introduction to solid-state physics related to device electronics, see R. S. Muller and T. I. Kamins, *Device Electronics for Integrated Circuits*, 2nd ed., (Wiley, Singapore, 1986).

[2] P. M. Fahey, P. B. Griffin, and J. D. Plummer, Rev. Mod. Phys. **61**, 289 (1989).

[3] J. Dabrowski, H.-J. Mussig, M. Duane, S. T. Dunham, R. Goossens, and H.-H. Vuong, Advances in Solid State Physics **38**, 565 (1999).

[4] A. Lietoila, J. F. Gibbons, and T. W. Sigmon, Appl. Phys. Lett. **36**, 765 (1980).

[5] P. A. Stolk, H.-J. Gossmann, D. J. Eaglesham, D. C. Jacobson, C. S. Rafferty, G. H. Gilmer, M. Jaraíz, J. M. Poate, H. S. Luftman, and T. E. Haynes, J. Appl. Phys. **81**, 6031 (1997).

[6] P. Hohenberg and W. Kohn, Phys. Rev. **136**, B864 (1964).

[7] W. Kohn and L. J. Sham, Phys. Rev. **140**, A1133 (1965).

[8] R. O. Jones and O. Gunnarsson, Rev. Mod. Phys. **61**, 689 (1989).

[9] N. W. Ashcroft and N. D. Mermin, *Solid State Physics*, (Saunders College Publishing, 1976), pp. 334-337.

[10] D. M. Ceperley and B. J. Alder, Phys. Rev. Lett. **45**, 566 (1980).

[11] J. P. Perdew and A. Zunger, Phys. Rev. B **23**, 5048 (1981).

[12] A. R. Williams and U. von Barth in *Theory of the Inhomogeneous Electron Gas*, edited by S. Lundqvist and N. H. March (Plenum, New York, 1983), pp. 189-308.

[13] L. Hedin, Phys. Rev. **139**, A796 (1965).

[14] B. M. Bylander and L. Kleinman, Phys. Rev. B **41**, 7868 (1990); A. Seidl, A. Görling, P. Vogl, J. A. Majewski, and M. Levy, *ibid.* **53**, 3764 (1996).

[15] M. C. Payne, M. P. Teter, D. C. Allan, T. A. Arias, and J. D. Joannopoulos, Rev. Mod. Phys. **64**, 1045 (1992).

[16] Computer code FINGER; a massively-parallel implementation of the plane-wave pseudopotential method. See S. Pöykkö, Ph.D. thesis, Laboratory of Physics, Helsinki University of Technology, 1998.

[17] M. Fuchs and M. Scheffler, Comput. Phys. Commun. **119**, 67 (1999), and references therein.

[18] D. Vanderbilt, Phys. Rev. B **41**, 7892 (1990); K. Laasonen, A. Pasquarello, R. Car, C. Lee, and D. Vanderbilt, *ibid.* **47**, 10142 (1993).

[19] S. G. Louie, S. Froyen, and M. L. Cohen, Phys. Rev. B **26**, 1738 (1982).

[20] The second-order damped dynamics and William-Soler algorithms are used in the electronic minimization. See F. Tassone, F. Mauri, and R. Car, Phys. Rev. B **50**, 10561 (1994); A. Williams and J. Soler, Bull. Am. Phys. Soc. **32**, 562 (1986); J. S. Nelson, S. J. Plimpton, and M. P. Sears, Phys. Rev. B **47**, 1765 (1993).

[21] A Broyden-Fletcher-Goldfarb-Shanno type algorithm is used in the ionic minimization. See W. H. Press, S. A. Teukolsky, W. T. Vetterling, and B. P. Flannery, *Numerical Recipes*, 2nd ed., (Cambridge University Press, 1992).

[22] See, for example, P. Y.Yu and M. Cardona, *Fundamentals of Semiconductors*, (Springer, Berlin, Heidelberg, 1996), p. 172.

[23] S. B. Zhang and J. E. Northrup, Phys. Rev. Lett. **67**, 2339 (1991).

[24] J. E. Northrup and S. B. Zhang, Phys. Rev. B **47**, 6791 (1993).

[25] A. Garcia and J. E. Northrup, Phys. Rev. Lett. **74**, 1131 (1995).

[26] S. Pöykkö, M. J. Puska, and R. M. Nieminen, Phys. Rev. B **53**, 3813 (1996).

[27] G. Makov and M. C. Payne, Phys. Rev. B **51**, 4014 (1995).

[28] *Positron Spectroscopy of Solids*, edited by A. Dupasquier and A. P. Mills, Jr. (IOS, Amsterdam, 1995).

[29] K. Saarinen, P. Hautojärvi, and C. Corbel, in *Identification of Defects in Semiconductors*, edited by M. Stavola (Academic Press, New York, 1998), p. 209.

[30] M. J. Puska and R. M. Nieminen, Rev. Mod. Phys. **66**, 841 (1994).

[31] B. Bergersen, E. Pajanne, P. Kubica, M. J. Stott, and C. H. Hodges, Solid State Commun. **15**, 1377 (1974).

[32] E. Boroński and R. M. Nieminen, Phys. Rev. B **34**, 3820 (1986); see also Ref. [33].

[33] M. J. Puska, A. P. Seitsonen, R. M. Nieminen, Phys. Rev. B. **52**, 10947 (1995).

[34] L. Lantto, Phys. Rev. B. **36**, 5160 (1987).

[35] J. Arponen and E. Pajanne, Ann. Phys. (N.Y.) **121**, 343 (1979); J. Phys. F **9**, 2359 (1979).

[36] A. P. Seitsonen, M. J. Puska, and R. M. Nieminen, Phys. Rev. B **51**, 14057 (1995).

[37] T. Korhonen, M. J. Puska, and R. M. Nieminen, Phys. Rev. B **54**, 15016 (1996).

[38] H. L. Skriver, *The LMTO Method* (Springer, New York, 1984).

[39] M. J. Puska and R. M. Nieminen, J. Phys. F **13**, 333 (1983).

[40] B. Barbiellini, M. J. Puska, T. Torsti, and R. M. Nieminen, Phys. Rev. B **51**, 7341 (1995); B. Barbiellini, M. J. Puska, T. Korhonen, A. Harju, T. Torsti, and R. M. Nieminen, *ibid.* **53**, 16201 (1996).

[41] A. Rubaszek, Z. Szotek, W. M. Temmerman, Phys. Rev. B **58**, 11285 (1998).

[42] K. O. Jensen and A. B. Walker, J. Phys. F **18**, L277 (1988).

[43] S. Daniuk, M. Šob, and A. Rubaszek, Phys. Rev. B **43**, 2580 (1991), and references therein.

[44] A. Rubaszek, Z. Szotek, and W. M. Temmerman, Phys. Rev. B **61**, 10100 (2000).

[45] H. Sormann, Phys. Rev. B **54**, 4558 (1996).

[46] M. J. Puska, S. Pöykkö, M. Pesola, and R. M. Nieminen, Phys. Rev. B **58**, 1318 (1998).

[47] W.-C. Lee, S.-G. Lee, and K. J. Chang, J. Phys.: Condens. Matter **10**, 995 (1998).

[48] H. Kauppinen, C. Corbel, K. Skog, K. Saarinen, T. Laine, P. Hautojärvi, P. Desgarding, and E. Ntsoenzok, Phys. Rev. B **55**, 9598 (1997).

[49] Ref. [59] and references therein.

[50] D. J. Chadi and K. J. Chang, Phys. Rev. B **38**, 1523 (1988).

[51] See, for example, J. Kim, J. W. Wilkins, F. S. Khan, and A. Canning, Phys. Rev. B **55**, 16186 (1997).

[52] N. E. B. Cowern, G. Mannino, P. A. Stolk, F. Roozeboom, H. G. A. Huizing, J. G. M. van Berkum, F. Cristiano, A. Claverie, and M. Jaraíz, Phys. Rev. Lett. **82**, 4460 (1999).

[53] M. Ramamoorthy and S. T. Pantelides, Phys. Rev. Lett. **76**, 4753 (1996).

[54] K. C. Pandey, A. Erbil, G. S. Cargill III, R. F. Boehme, and D. Vanderbilt, Phys. Rev. Lett. **61**, 1282 (1988).

[55] G. D. Watkins, Phys. Rev. B **12**, 5824 (1975).

[56] J. R. Troxell and G. D. Watkins, Phys. Rev. B **22**, 921 (1980).

[57] G. D. Watkins and J. R. Troxell, Phys. Rev. Lett. **44**, 593 (1980).

[58] G. Watkins, Phys. Rev. B **13**, 2511 (1976).

[59] G. D. Watkins, in *Defects and Diffusion in Silicon Processing*, edited by T. Dias de la Rubia, S. Coffa, P. A. Stolk, and C. S. Rafferty, MRS Symposium Proceedings No. 469 (Materials Research Society, Pittsburgh, 1997), p. 139.

[60] V. V. Emtsev, P. Ehrhart, D. S. Poloskin, and U. Dedek, Physica B **273-274**, 287 (1999).

[61] C. S. Nichols, C. G. Van de Walle, and S. T. Pantelides, Phys. Rev. Lett. **62**, 1049 (1989); Phys. Rev. B **40**, 5484 (1989).

[62] N. E. B. Cowern, K. T. F. Janssen, G. F. A. van de Walle, and D. J. Gravesteijn, Phys. Rev. Lett. **65**, 2434 (1990).

[63] N. E. B. Cowern, G. F. A. van de Walle, D. J. Gravesteijn, and C. J. Vriezema, Phys. Rev. Lett. **67**, 212 (1991).

[64] N. E. B. Cowern, G. F. A. van de Walle, P. C. Zalm, and D. J. Oostra, Phys. Rev. Lett. **69**, 116 (1992).

[65] J. Zhu, T. D. Rubia, L. H. Yang, C. Mailhiot, and G. H. Gilmer, Phys. Rev. B **54**, 4741 (1996).

[66] J. Zhu, Comput. Mater. Sci. **12**, 309 (1998).

[67] B. Sadigh, T. J. Lenosky, S. K. Theiss, M.-J. Caturla, T. D. de la Rubia, and M. A. Foad, Phys. Rev. Lett. **83**, 4341 (1999).

[68] W. Windl, M. M. Bunea, R. Stumpf, S. T. Dunham, and M. P. Masquelier, Phys. Rev. Lett. **83**, 4345 (1999).

[69] A. E. Michael, W. Rausch, P. A. Ronsheim, R. H. Kastl, Appl. Phys. Lett. **50**, 416 (1987).

[70] N. E. B. Cowern, K. T. F. Janssen, H. F. F. Jos, J. Appl. Phys. **68**, 6191 (1990).

[71] L. Pelaz, M. Jaraíz, G. H. Gilmer, H.-J. Gossmann, C. S. Rafferty, D. J. Eaglesham, and J. M. Poate, Appl. Phys. Lett. **70**, 2285 (1997).

[72] L. Pelaz, G. H. Gilmer, H.-J. Gossmann, C. S. Rafferty, M. Jaraíz, and J. Barbolla, Appl. Phys. Lett. **74**, 3657 (1999).

[73] J. L. Benton, K. Halliburton, S. Libertino, D. J. Eaglesham, and S. Coffa, J. Appl. Phys. **84**, 4749 (1998).

[74] J. L. Benton, S. Libertino, P. Kringhøj, D. J. Eaglesham, J. M. Poate, and S. Coffa, J. Appl. Phys. **82**, 120 (1997).

[75] J. Kim, F. Kirchoff, J. W. Wilkins, and F. S. Khan, Phys. Rev. Lett. **84**, 503 (2000).

[76] Ref. [71], and references therein.

[77] P. A. Stolk, H.-J. Gossmann, D. J. Eaglesham, D. C. Jacobson, and J. M. Poate, Appl. Phys. Lett. **66**, 568 (1995).

[78] M. J. Caturla, M. D. Johnson, and T. D. de la Rubia, Appl. Phys. Lett. **72**, 2736 (1998).

[79] W. Windl, unpublished.

[80] E. Tarnow, J. Phys.: Condens. Matter **4**, 5405 (1992).

[81] P. Pluvinage, J. Phys. Radium **12**, 789 (1951); O. Dulieu and C. le Sech, Europhys. Lett. **3**, 975 (1987).

[82] D. D. Koelling and B. N. Harmon, J. Phys. C **10**, 3107 (1977).

[83] S. Dannefaer, W. Puff, D. Kerr, Phys. Rev. B, **55**, 2182 (1997).

[84] H. Kauppinen and K. Saarinen (private communication).

[85] J. Mäkinen, P. Hautojärvi, and C. Corbel, J. Phys. Condens. Matter **4**, 5137 (1992).

[86] S. Eichler and R. Krause-Rehberg, Appl. Surf. Sci., **149**, 227 (1999).

[87] L. Liszkay, K. Havancsák, and Zs. Kajcsos, Appl. Surf. Sci., **149**, 181 (1999).

[88] J. Mäkinen, C. Corbel, P. Hautojärvi, P. Moser, and F. Pierre, Phys. Rev. B **39**, 10162 (1989).

[89] D. Mathiot and J. C. Pfister, Appl. Phys. Lett. **42**, 1043 (1983).

[90] O. Gunnarsson and B. I. Lundqvist, Phys. Rev. B **13**, 4274 (1976).

[91] R. D. Harris, J. L. Newton, and G. D. Watkins, Phys. Rev. B **36**, 1094 (1987).